Free Radical Research, 2014; Early Online: 1–15

ISSN 1071-5762 print/ISSN 1029-2470 online
DOI: 10.3109/10715762.2014.906592

informa
healthcare

ORIGINAL ARTICLE

Abnormal mitochondrial fusion–fission balance contributes to the progression of experimental sepsis

A. S. Gonzalez[1,2], M. E. Elguero[1], P. Finocchietto[1], S. Holod[2], L. Romorini[3], S. G. Miriuka[3], J. G. Peralta[1], J. J. Poderoso[1] & M. C. Carreras[1,2]

[1]*Laboratory of Oxygen Metabolism, University of Buenos Aires, INIGEM-CONICET, Buenos Aires, Argentina,* [2]*Department of Clinical Biochemistry, School of Pharmacy and Biochemistry, INFIBIOC, University of Buenos Aires, Buenos Aires, Argentina, and* [3]*Laboratorio de Biología del Desarrollo Celular, LIAN, FLENI, Buenos Aires, Argentina*

Abstract

Sepsis-associated multiple organ failure is a major cause of mortality characterized by a massive increase of reactive oxygen and nitrogen species (ROS/RNS) and mitochondrial dysfunction. Despite intensive research, determining events in the progression or reversal of the disease are incompletely understood. Herein, we studied two prototype sepsis models: endotoxemia and cecal ligation and puncture (CLP)—which showed very different lethality rates (2.5% and 67%, respectively)—, evaluated iNOS, ROS and respiratory chain activity, and investigated mitochondrial biogenesis and dynamics, as possible processes involved in sepsis outcome. Endotoxemia and CLP showed different iNOS, ROS/RNS, and complex activities time-courses. Moreover, these alterations reverted after 24-h endotoxemia but not after CLP. Mitochondrial biogenesis was not elicited during the first 24 h in either model but instead, 50% mtDNA depletion was observed. Mitochondrial fusion and fission were evaluated using real-time PCR of mitofusin-2 (Mfn2), dynamin-related protein-1 (Drp1), and using electron microscopy. During endotoxemia, we observed a decrease of Mfn2-mRNA levels at 4–6 h, and an increase of mitochondrial fragmentation at 6 h. These parameters reverted at 24 h. In contrast, CLP showed not only decreased Mfn2-mRNA levels at 12–18 h but also increased Drp1-mRNA levels at 4 h, and enhanced and sustained mitochondrial fragmentation. The *in vivo* pretreatment with mdivi-1 (Drp1 inhibitor) significantly attenuated mitochondrial dysfunction and apoptosis in CLP. Therefore, abnormal fusion-to-fission balance, probably evoked by ROS/RNS secondary to iNOS induction, contributes to the progression of sepsis. Pharmacological targeting of Drp1 may be a potential novel therapeutic tool for sepsis.

Keywords: nitric oxide, mitochondria, lipopolysaccharide, reactive oxygen species, iNOS

Introduction

Sepsis and multiple organ failure remain a leading cause of mortality. The events triggered early in the onset of human sepsis seem to be crucial in the prognosis of the disease. Early diagnosis and interventions have been documented to improve outcomes and decrease sepsis-related mortality when implemented in the initial "golden hours" [1].

Preclinical models cannot fully replicate the complexity of human sepsis [2,3]. The simplest animal model of sepsis involves the exogenous administration of a toxin, such as bacterial lipopolysaccharide (LPS) [4,5]. Other sepsis models are based on the disruption of the intestinal barrier by surgical procedures; among them, cecal ligation and puncture (CLP) is the most frequently used model. Endotoxin administration mimics blood bacterial contamination or transient episodes of bacteriemia compared to that of fecal peritonitis, which depicts sepsis after a more complex and severe clinical picture that leads to multiple organ failure [6].

During sepsis, the liver is the second organ affected after the lungs, and plays a major function in host defense [7], clearing circulating bacteria and bacterial products, and producing acute-phase reactants. These include tumor necrosis factor-α (TNF-α) and interleukins (IL), which call the pro-inflammatory network to action, including inducible nitric oxide synthase (iNOS) [8,9].

Nitric oxide (NO) is an important element of host defense, a central component of innate immunity, and an effective antimicrobial agent [10]. Large amounts of NO and peroxynitrite ($ONOO^-$), among other factors, are implicated as mediators for the late phase of hypotension, apoptosis, lactic acidosis, and multiple organ failure in septic or endotoxic shock [8,9]. Mitochondrial dysfunction and the subsequent disruption in energy metabolism are associated with multiple organ failure, and an increased mortality in critically ill patients [11]. Oxidative/nitrosative stress occurs within the mitochondria during sepsis. Persistent high levels of NO and other free radicals, result in mitochondrial proteins (semi-) permanent modifications, particularly affecting complex I [12], leading to a prolonged inhibition of mitochondrial respiration and, subsequently, to the decline of ATP synthesis. Besides proteins, other molecules such as phospholipids and nucleic acids are vulnerable to oxidative/nitrosative stress. Indeed, mitochondrial DNA is particularly susceptible,

Correspondence: Prof. María Cecilia Carreras, PhD, Laboratory of Oxygen Metabolism, University of Buenos Aires, INIGEM-CONICET, Córdoba 2351, C1120AAR- Buenos Aires, Argentina. Tel/Fax: + 54-11-5950-8365. E-mail: carreras@ffyb.uba.ar

(Received date: 22 October 2013; Accepted date: 17 March 2014; Published online: 10 April 2014)

due to its naked structure and proximity to free radicals production site undergoing degradation, which results in incomplete synthesis of respiratory chain proteins and exacerbation of reactive oxygen species (ROS) generation. However, oxidative stress is not only associated with mitochondrial DNA depletion, but also with increased mtDNA content, like in aging and exercise, which could be understood as a regulatory mechanism that prevents cell energy deprivation [13]. In this context, increased mitochondrial biogenesis is part of the cellular response to oxidative stress [14]. The mtDNA transcription and replication are regulated by nuclear factors and co-activators such as peroxisome proliferator-activated receptor gamma coactivator 1-alpha (PGC-1α), nuclear respiratory factors (NRF) 1 and 2, and the mitochondrial transcription factor A (Tfam) [15].

Oxidative stress also results in mitochondrial fragmentation [16]. Mitochondrial fusion through mitofusins (Mfn) 1 and 2, and optic atrophy 1 (OPA1) and fission through dynamin-related protein 1 (Drp1), fission 1 (Fis1), and mitochondrial fission factor work in concert to maintain the shape, size, and number of mitochondria and their physiological function [17,18]. The balance of these opposing events affects the inheritance of mtDNA, transmission of energy, cellular differentiation, metabolite maintenance, and calcium homeostasis [19]. The dynamic process is thought to function as a rescue mechanism: fusion allows dysfunctional/damaged mitochondria to recover its functionality by coupling to healthy ones; fission induces fragmentation of the organelle and mitophagy when damage is excessive, in order to rescue the cell [16–19]. If this is not possible, apoptosis or necrosis signal take over and execute cell death. In spite of its protective role, excessive mitochondrial fission is associated with neurodegeneration and other mitochondriopathies. Recently, an inhibitor of Drp1, mitochondrial division inhibitor (mdivi-1), which blocks the self-assembly of Drp1, and protects against different pathological situations as ischemic renal, brain, or myocardial damage *in vivo*, has been described [20].

In this context, the aim of this study is to evaluate mitochondrial biogenesis and dynamics in relation to mitochondrial nitro-oxidative stress as possible processes involved in sepsis outcome, performing endotoxemia and CLP models as experimental approaches.

Methods

Chemicals

Griess assay kit was purchased from Cayman (Ann Harbor, MI). The Oxyblot detection kit, ApopTag® Plus In Situ Apoptosis Fluorescein detection kit and Fluorsave were from Millipore (Billerica, MA). Proteinase K, 4-amino-5-methylamino-2′,7′-difluorofluorescein diacetate (DAF-FM diacetate), DMEM, Mitotracker green, Trizol, Alexa Fluor conjugated anti-rabbit IgG and SYBR® GreenER™ qPCRSuperMix, from Invitrogen (Carlsbad, CA). Antibodies against iNOS (M19), Tom 40, VDAC, cytochrome c and β-actin were from Santa Cruz (Santa Cruz, CA); against 3-nitrotyrosine (clone 1A6), from Upstate-Millipore (Bedford, MA). Horseradish peroxidase-conjugated secondary antibodies and ECL immunochemical detection kit were obtained from GE Healthcare (Piscataway, NJ, USA). The 3 H-L-arginine was from Perkin Elmer (Waltham, MA) and M-MLV reverse transcriptase from Promega (Madison, WI). LPS from Escherichia *coli*, O153, 2′,7′-dichlorodihydrofluorescein-diacetate (DCFH-DA), 1400 W, L-N^G-nitroarginine methyl ester (L-NAME), mitochondrial division inhibitor (mdvi-1), and other chemicals were purchased from Sigma-Aldrich (St. Louis, MO).

Animals

Male Wistar rats (3 months old, 220–250 g) were purchased from the School of Pharmacy and Biochemistry, University of Buenos Aires, Argentina. Animal experiments were performed in accordance with the Principles of Laboratory Animal Care. The animal experiments were approved by the local Scientific and Technology Ethics Committee at the University of Buenos Aires. All efforts were made to minimize animal suffering and to reduce the number of animals used. For endotoxemic model, Wistar rats were injected i.p. with 10 mg/kg body weight of LPS from Escherichia coli, O153, and sacrificed at 2, 4, 6, 12, and 24 h. Control animals were injected with sterile pyrogen-free 0.9% sodium chloride. For the CLP model, animals were fasted for 16 h before any surgical procedure. Rats were anesthetized with ketamine and xylazine (60 and 7.5 mg/kg body weight, respectively), and subjected to cecal ligation-double puncture procedure with a 21-gauge needle as described [6]. Sham group was subjected to the same procedure avoiding CLP. After surgery, 5 ml of 0.9% saline was injected subcutaneously to prevent shock. Animals were sacrificed at 2, 4, 6, 12, and 18 h after the procedure. Animals were randomly assigned for each group and each experimental model.

Drug administration and experimental groups

Rats were randomly divided in four treatment groups: sham + DMSO, sham + mdivi-1, CLP 18 h + DMSO, and CLP 18 h + mdvi-1. Mdivi-1 was injected at 50 mg/kg intraperitoneally (dissolved in DMSO) 1 h prior to sham or CLP procedure and animals were sacrificed at 18 h after surgery. Additionally, CLP and sham rats injected with DMSO alone were included [20].

Biochemical parameters

Blood samples were collected using cardiac puncture. Nitrite/nitrate concentrations (NOx) were determined by Griess assay, oxidation and nitration of plasma proteins by Oxyblot detection kit and immunoblotting against 3-nitrotyrosine, respectively, and chemical determinations were done by standard methods.

Isolation and Purification of Liver Mitochondria

Liver mitochondria were isolated from homogenized tissue by differential centrifugation. When needed, further purification was performed using Percoll gradient, as described [21]; minimal contamination was found (2–3%) by comparing activities of lactate dehydrogenase (cytosolic marker) and succinate-cytochrome c reductase (mitochondrial marker). Mitochondrial pellets were stored in the presence of antiproteases and antiphosphatases. For mitochondrial treatment with 50 μg/ml proteinase K, antiproteases were avoided.

Preparation of mitochondrial fractions

Fractionation of purified mitochondria was performed using hypotonic disruption and differential centrifugation, as previously described [22]. Briefly, mitochondria were broken by water treatment and centrifuged at 12,000 g at 4°C for 10 min; supernatant represents outer membrane and intermembrane space (OM + IMS) and pellet, mitoplasts (MP). Supernatant was centrifuged at 100,000 g for 30 min to precipitate OM. Mitoplasts were further disrupted by sonication, and centrifuged at 8000 g to discard unbroken mitoplasts; supernatant was centrifuged at 100 000 g for 30 min. Supernatant represents matrix fraction (M) and pellet, inner membrane fraction (IM). Purity of the fractions was tested using immunoblotting of proteins specifically localized in each fraction: Tom40, cytochrome c, VDAC, and MnSOD for OM, IMS, IM, and M, respectively.

Immunoblotting

Proteins were separated using electrophoresis on 7.5% (iNOS, 3-nitrotyrosine and carbonyl groups) or 10% (β-actin and Tom40) SDS-polyacrylamide gel, as appropriated and transferred to a PVDF membrane (GE, Healthcare). Membranes were incubated with antibodies anti-iNOS (M19, 1:1000), Tom 40 (1: 10000), and β-actin (1:3000), and, after several washes, incubated with appropriate horseradish peroxidase-conjugated secondary antibodies. Detection of immunoreactive proteins was accomplished by chemiluminescence with ECL. Quantification of bands was performed by digital image analysis by Totallab analyzer software (Nonlinear Dynamics Ltd, Biodynamics, Argentina). Equal loading was controlled with the appropriate subcellular markers.

NOS activity in subcellular fractions

NOS activity was determined in mitochondrial and cytosolic fractions by conversion of [^{3}H]-L-arginine to [^{3}H]-L-citrulline as previously described [21]. Inducible NOS activity was calculated by the subtraction of the activity measured in the presence of its specific inhibitor 1400 W.

Immunogold electron microscopy

Purified mitochondria were suspended in 4% paraformaldehyde and 0.5% glutaraldehyde, pH 7.4, for 2 h at 4°C, washed overnight with 0.32 M sucrose at 4°C, further dehydrated and embedded in Vestopal. Immunocytochemistry was performed using a primary polyclonal antibody anti-C-terminal iNOS at a dilution of 1:20 in phosphate-buffered saline (PBS), pH 7.4, and a gold-coupled goat secondary antibody. Grids were washed in PBS and counterstained with 1% uranyl acetate. Nonspecific background was blocked by incubation with 5% normal goat serum in PBS at the beginning of the procedure. Positive (using cytochrome c as primary antibody) and negative controls (in the absence of a primary antibody) were included. Specimens were observed in a Zeiss EM-109-T transmission electron microscope (Zeiss, Oberkochen, Germany) at 80 kV.

Liver Cell Isolation and Detection of Intracellular oxidants

Hepatocytes were isolated using two-step collagenase perfusion [23]. Intracellular oxidants were detected using flow cytometry after incubating hepatocytes in phenol red-free DMEM with 5 μM DCFH-DA for 30 min, at 37°C with 5% CO_2.

Confocal microscopy

Hepatocytes were grown on glass coverslips, and fixed for 20 min with cold paraformaldehyde 2%. Following rehydration with PBS, cells were permeabilized with 0.1% Triton X-100 and blocked with 3% fetal bovine serum, each for 30 min. Cells were incubated with antibodies directed against Tom 40 and iNOS (1:100 dilution) overnight at 4°C, washed with PBS, and exposed to goat Alexa Fluor 488 conjugated anti-rabbit IgG for Tom 40 staining, and goat Alexa Fluor 594-conjugated anti-mouse IgG for iNOS (1:500 dilution) for 45 min. After extensive rinsing with PBS, samples were incubated with diamidinophenylindole (0.5 μg/ml), mounted with Fluorsave. Samples were kept at 4°C prior to analysis. Detection was performed using confocal microscopy Olympus FV300 (Olympus Ltd, Tokyo, Japan). For negative controls, an identical procedure was followed, but primary antibodies were omitted (data not shown).

Detection of mitochondrial nitric oxide

Mitochondria (1 mg protein/ml) were incubated with 10 μM of DAF-FM, 0.5 μM of Mitotracker green, and 0.3 mM of L-arginine for 30 min, at 37°C in a humidified incubator under an atmosphere equilibrated with 5% CO_2. Other mitochondrial fractions were preincubated with 3 mM NOS inhibitor L-NAME during 30 min before dye incubation to determine unspecific fluorescence. Fluorescence was measured with a FACScalibur Flow-Cytometer (Becton-Dickinson, Mountain View, CA) [24].

Mitochondrial electron transfer chain complex activities

Disrupted mitochondria were prepared by three cycles of freezing/thawing. Nicotinamide adenine dinucleotide— and succinate-cytochrome *c* reductase activities

(complexes I–III and II and III, respectively) were assayed by cytochrome *c* reduction at 550 nm with a Hitachi U3000 spectrophotometer (Hitachi, Tokyo, Japan) at 30°C. Cytochrome oxidase activity (Complex IV) was determined by monitoring cytochrome *c* oxidation at 550 nm ($\varepsilon_{550} = 21\ mM^{-1}.cm^{-1}$); the reaction rate was measured as the pseudo–first-order reaction constant (*k'*) and expressed as *k'*/min. mg protein [25].

Genomic DNA preparation

Liver material was homogenized in lysis buffer (10 mM Tris-HCl pH 8, 1 mM EDTA, and 0.1% SDS). After adding proteinase K, lysates were incubated at 55°C for 3 h, vortexed vigorously and centrifuged (8000 g for 15 min); the resting supernatant was mixed with phenol/chloroform/isoamyl alcohol (25:24:1), and centrifuged. The supernatant was vigorously mixed with chloroform and centrifuged (8000 g for 15 min); the resulting supernatant was mixed with sodium acetate and isopropanol. Tube was maintained at − 20°C for 10 min and then centrifuged. The DNA pellets were washed with 70% ethanol, air dried, and dissolved in Tris-EDTA buffer. Genomic DNA stock was subsequently diluted in DNAse-free water to a final concentration of 40 ng/µl.

RNA isolation and Retrotranscription

Total RNA was extracted from liver with Trizol. The cDNA was synthesized from 1 µg of total RNA with 15 mM of random hexamers and MMLV reverse transcriptase according to manufacturer's instructions.

Quantitative real-time PCR (RT-qPCR)

For RT-qPCR studies, cDNA samples were diluted 5-fold, and, for mtDNA/nDNA qPCRs, 40 ng of total genomic DNA were used. PCR amplification and analysis were performed with ABI PRISM 7500 Sequence Detector System (PE Applied Biosystems, Foster City, CA). The SYBR® GreenER™ qPCR SuperMix UDG was used for all reactions, following manufacturer instructions. The mtDNA/nDNA ratio was calculated using mtDNA primers for the D-loop region and primers for a single-copy nuclear gene (glyceraldehyde 3-phosphate dehydrogenase, GAPDH) that is assumed to be present in two copies per diploid genome. The primer sequences and sizes of the amplified fragments are shown in Table I.

Electron microscopy

Liver samples were fixed in 4% paraformaldehyde, 2% glutaraldehyde, and 5% sucrose in PBS, followed by 2-h post-fixation in 1% osmium tetroxide, and then 1 h in uranyl acetate in 50% ethanol. Samples were washed with ethanol 50% and dehydrated with a graded series of ethanol, clarified with acetone and embedded in Vestopal. Grids were prepared and stained with uranyl acetate and lead citrate. Samples were observed at 100 kV with a Zeiss EM-109-T transmission electron microscope (Zeiss, Oberkochen, Germany).

Table I. Rat gene-specific oligonucleotide sequences used in quantitative real-time polymerase chain reaction.

Gene product	Primer sequences
Mfn2	FW: 5′-GCACCGCCATATAGAGGAAGG-3′ RV: 5′-CGCACAGACACAGGAAGAAGG-3′
Drp1	FW: 5′-GACTTTGCTGATGCCTGTGG-3′ RV: 5′-GTTGCCTGTTGTCGGTTCC-3′
PGC-1α	FW: 5′-CACAACCGCAGTCGCAAC-3′ RV: 5′-TGGCTTTATGAGGAGGAGTCG-3′
NRF1	FW: 5′-AGTATGCTAAGTGCTGATGAAG-3′ RV: 5′-AACCGTGTCTGCTGTCTC-3′
NRF2	FW: 5′-GAGCAAGTGACGAGATGG-3′ RV: 5′-AATGTTGAGTGTGGTGAGG-3′
Tfam	FW: 5′-CCTCGGTCAGCATATAAC-3′ RV: 5′-CTTCATTTCATTGTCATAACG-3′
β-actin	FW: 5′-CACACCCGCCACCAGTTC-3′ RV: 5′-CCCATACCCACCATCACACC-3′
D-loop	FW: 5′-TGGTAAAATTTCCCGACACA-3′ RV: 5′-ATAAGGCCAGGACCAAACCT-3′
GAPDH	FW: 5′-AGACAGCCGCATCTTCTTGT-3′ RV: 5′-TGATGGCAACAATGTCCACT-3′

Mfn2, mitofusin 2; Drp1, dynamin-related protein 1; PGC-1α, peroxisome proliferator-activated receptor-γ-coactivator-1α; NRF1, nuclear respiratory factor 1; NRF2, nuclear respiratory factor 2; Tfam, mitochondrial transcription factor A; GADPDH, glyceraldehyde 3-phosphate dehydrogenase; FW, forward; RV, reverse.

Terminal deoxynucleotidyltransferase-mediated dUTP nick-end labeling (TUNEL) assay

Liver samples were fixed in 10% paraformaldehyde and embedded in paraffin, and then liver slices were taken and processed according to Apop Tag Plus detection kit.

Statistical analysis

Data are mean ± SEM. Survival rate was tested using Log-rank test. Other parameters were tested using One-way analysis of variance with *post-hoc* Dunnett's or Bonferroni test, and significance were accepted at $P < 0.05$. The GraphPad Prism 5.0 (La Jolla, CA) program was used for both statistical analysis and figure design.

Results

Survival rates in endotoxemia and CLP

Survival rates were very similar for both models until 12 h after each procedure, but afterwards, mortality abruptly increased in CLP (67.1% vs. 2.5% at 24 h) (Supplementary Figure 1 available online at http://informahealthcare.com/doi/abs/10.3109/10715762.2014.906592). In this context, the observations stopped at 24 h, and we studied the time course of CLP up to 18 h after surgery.

We also tested biochemical parameters in order to evaluate hepatic, renal, and muscle damage (Supplementary

Table I available online at http://informahealthcare.com/doi/abs/10.3109/10715762.2014.906592). Hepatic transaminases—alanine transaminase (ALT) and aspartate transaminase (AST)—, urea, lactate dehydrogenase (LDH), and creatine kinase (CK) were significantly increased by 2–3 fold after 6–12 h LPS, but returned to control values at 24 h. In contrast, almost all parameters were markedly increased after 12–18 h CLP.

These data showed that biochemical alterations were reverted after 24 h of LPS treatment, while CLP induced a progressive and irreversible impairment leading to multiple organ failure and death.

iNOS time course in liver mitochondria

During endotoxemia, iNOS expression and activity progressively increased in cytosol since 2 h up to 6 h after LPS inoculation, and then decreased (Figure 1A and B). iNOS translocated into mitochondria reached its maximal expression at 6 h, which was maintained even after proteinase K treatment, indicating the intramitochondrial localization of the enzyme. Interestingly, mitochondrial import was not dependent on the levels of iNOS cytosolic expression, since at 4 h mitochondrial expression was very low while cytosolic expression was almost maximal, suggesting a regulated mechanism for iNOS import. Time course of iNOS expression and activity in CLP was different to LPS one, because it progressively increased at 12–18 h, in both cytosol and mitochondrial compartments and, in opposite to endotoxemia, it did not return to control (sham) levels. No modulation was observed in Ca-dependent mtNOS activity or expression in either experimental model (data not shown).

Mitochondrial fractionation showed that iNOS was mainly present at the outer mitochondrial membrane and in the intermembrane space after proteinase K incubation in 6-h LPS-treated rats (Figure 1C).

Mitochondrial expression of iNOS was also demonstrated using immunogold electron microscopy (Figure 1D) and confocal microscopy (Figure 2). Interestingly, in CLP, perinuclear clustering of mitochondria was observed using confocal microscopy.

Nitrative and oxidative stress time course

Mitochondrial NO levels were measured using flow cytometry with DAF-FM dye in the presence or absence of the NOS inhibitor, L-NAME. As shown in Figure 3. A, maximal NO detection was at 4–6 h (6-fold respect to control), and then decreased at 24 h in LPS, while it was maximal at 12–18 h in CLP (3-fold respect to sham), in parallel to iNOS expression.

Oxidants production was measured in isolated hepatocytes using flow cytometry with DCFH-DA at different times after each treatment. The data showed a similar pattern to mitochondrial NO production in both experimental models (Figure 3B).

Protein carbonyls and nitration in liver mitochondria were also maximal at 4–6 h after LPS treatment and 12 h after CLP (Figure 3C and D).

Plasma protein oxidation and nitration were also evaluated (Supplementary Figure 2A available online at http://informahealthcare.com/doi/abs/10.3109/10715762.2014.906592), showing maximal band intensities at 12 h in endotoxemia and CLP. NO metabolites nitrate and nitrite (NOx) were significantly increased only at 6 h of LPS treatment, but from 6 to 18 h after CLP (Supplementary Figure 2B available online at http://informahealthcare.com/doi/abs/10.3109/10715762.2014.906592).

ETC complex activities

As nitro-oxidative stress compromises mitochondrial function and the respiratory chain, we evaluated the activity of the electron transfer chain (ETC) complexes (Figure 4). As expected, we observed impairment of mitochondrial functionality that paralleled ROS/RNS overproduction. In LPS, there was a significant inhibition of the activities of complexes I–III (−65% at 4–12 h) and complex IV (−50% at 6–12 h); this effect reverted at 24 h (Figure 4A and C). Complexes II and III were not affected (Figure 4B). In contrast, CLP resulted in a progressive decrease of the activity of all the assessed mitochondrial complexes (up to 50–60% inhibition), and no reversion was observed. Alterations of systemic biochemical parameters were also in accordance with this time course (Supplementary Table I available online at http://informahealthcare.com/doi/abs/10.3109/10715762.2014.906592).

Liver mitochondrial biogenesis

As mitochondrial biogenesis is part of the cellular response to oxidative stress, and it is addressed by some authors to mediate mitochondrial recovery, we studied transcriptional activation of nuclear-encoded activators by RT-qPCR and mtDNA/nDNA levels (Figure 5). An mRNA analysis of PGC-1α showed a 4-fold increase at 2 h after LPS administration and then a decrease to less than 50% at 4–12 h; while after CLP there was about a 4-fold increase at 2–4 h and then, a progressive decrease (Figure 5A). The mRNA profile of the transcription factor NRF1 showed only a significant increase (2-fold) at 6 h after LPS treatment (Figure 5B), and NRF2 mRNA had nonsignificant modifications in either experimental model (Figure 5C). Transcription factor, Tfam, was negatively modulated in both models with a significant decrease at 6–24 h after LPS and 12–18 h after CLP (about 50–60%) (Figure 5D). Because mtDNA damage can impair mitochondrial gene transcription, mtDNA content was evaluated using real-time PCR (Figure 5E). As expected, mtDNA/nDNA ratio was diminished after either treatment (−50%). These data indicate that mitochondrial biogenesis is not involved in mitochondrial and systemic recovery at 24 h after endotoxemia.

Liver mitochondrial dynamics

We then measured the transcriptional regulation of mitochondrial fusion and fission proteins Mfn2 and Drp1,

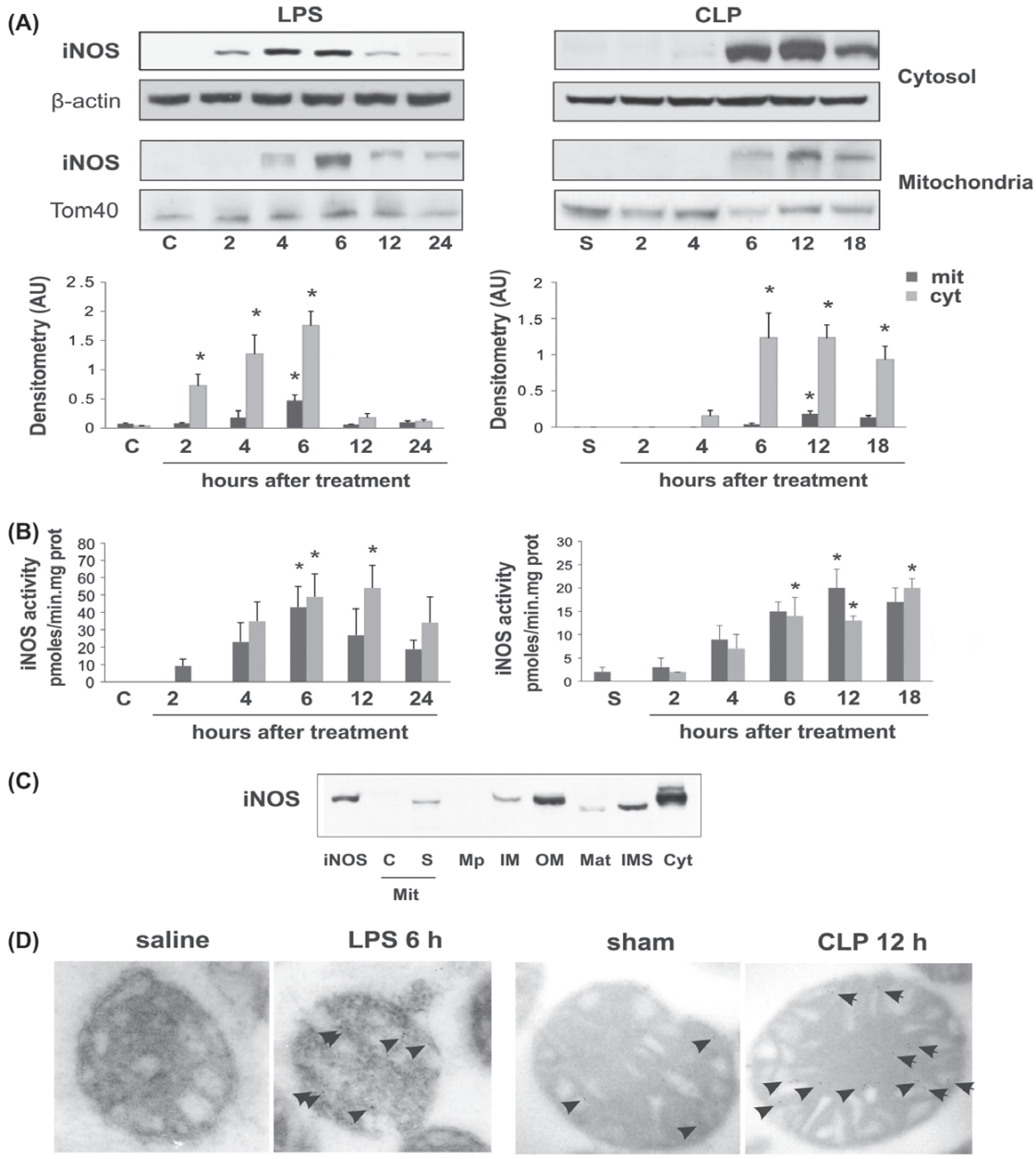

Figure 1. iNOS expression and activity in experimental sepsis. Rats were sacrificed at 2, 4, 6, 12, and 24 h after LPS administration (10 mg/kg) and at 2, 4, 6, 12, and 18 h after CLP procedure. Control rats were treated with pyrogen-free saline solution and sham rats were subjected to a midline laparotomy as CLP group but avoiding cecal ligation and puncture. (A) Representative immunoblot of proteins separated using SDS-PAGE reveals the differential distribution of iNOS in cytosol and mitochondria of rat livers at different times after treatment ($n = 5$, for each experimental group). (B) Time course of iNOS activity in cytosol and mitochondria of rat livers measured by 3H-L-citrulline formation ($n = 6$, for each experimental group, per duplicate). (C) Submitochondrial distribution of iNOS obtained from rat liver after 6 h of LPS treatment. Abbreviations: iNOS: positive control; C: control mitochondria; S: mitochondria from LPS-treated animals; Mp: mitoplasts; IM: inner mitochondrial membrane; OM: outer mitochondrial membrane; Mat: matrix; IMS: intermembrane space and Cyt: cytosol from LPS-treated animals ($n = 3$). Values represent means ± standard error of the mean (SEM), *represents $p < 0.05$ respect to control or sham, one-way analysis of variance (ANOVA) and Dunnett's post-hoc test. (D) Representative immunogold electron microscopy of control and 6 h LPS (on the left), and sham and 12 h CLP rat liver mitochondria (on the right) against polyclonal C-terminal iNOS antibody (primary magnification: 40,000×) from $n = 3$ for each experimental group.

respectively. Endotoxemia showed a significant decrease of Mfn2 mRNA at 4–6 h (~70–80%), and no changes of Drp1 mRNA. On the other hand, CLP evolved with a significant decrease of Mfn2 mRNA after 12 h (~60%), and a significant increase of Drp1 mRNA at 4 h (2-3 folds), (Figure 6A and B).

Electron microscopy of rat liver slices showed some morphological changes in mitochondria that were quantified

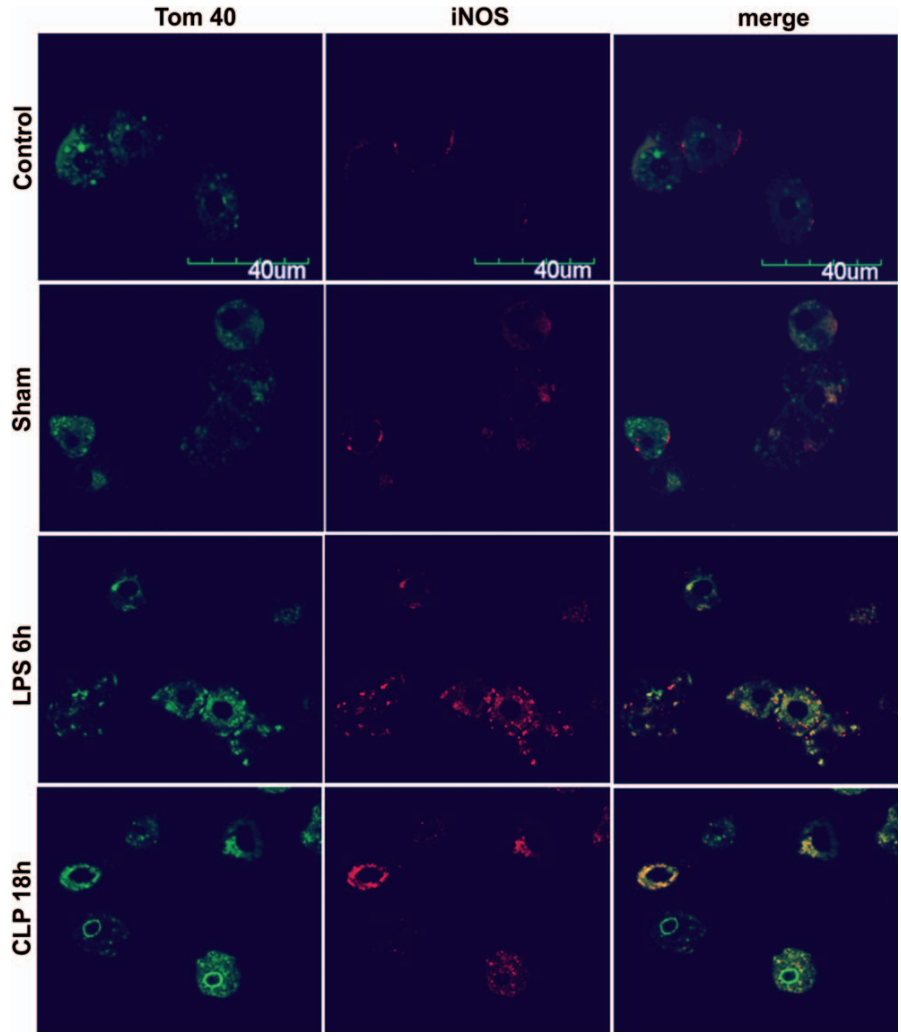

Figure 2. Colocalization of iNOS with Tom40 in hepatocytes of septic rats. Rats were sacrificed after 6 h of LPS administration (10 mg/kg) and at 18 h after CLP procedure. Hepatocytes were isolated using two-step collagenase perfusion and then grown on glass coverslips, and fixed with paraformaldehyde 2%. Cells were incubated with antibodies directed against Tom40 and iNOS and then exposed to goat Alexa Fluor 488 conjugated anti-rabbit IgG for Tom40 staining, and goat AlexaFluor 594-conjugated anti-mouse IgG for iNOS ($n = 3$, per duplicate).

per arbitrary area. Control and sham groups were characterized by predominantly tubular-shaped mitochondria. At 6 h of LPS treatment, time point of maximal ROS damage, tubular mitochondria decreased (−45%), and round-shaped mitochondria increased (+46%). It occurred simultaneously to the diminution of Mfn2 mRNA. At 24 h, when mitochondria functionality recovered, the differential percentage of mitochondrial shapes returned to that of control group (Figure 6C). On the other hand, at 12 h of CLP surgery, tubular mitochondria were decreased (−65%) and round (fragmented) ones were increased (+100%) (Figure 6D). In contrast to LPS treatment, after CLP procedure, no reversion of this effect was observed.

Taking into account that mitochondrial fragmentation could be related to apoptosis by the mitochondrial-mediated pathway, we evaluated apoptosis by TUNEL assay (Figure 7). We observed increased positive cells in endotoxemia at 6 h, which reverted at 24 h, and in CLP at 12–18 h, indicative of apoptosis, suggesting that increased mitochondrial fragmentation resulted in cell apoptosis in sepsis.

Effects of pharmacological inhibition of Drp1 on CLP

In order to investigate the effect of the inhibition of mitochondrial fission on the progressive mitochondrial dysfunction observed in CLP, we pretreated rats with mdivi-1, the selective Drp1 GTPase activity inhibitor. Electron microscopy of liver slices confirmed that intraperitoneally injected mdivi-1 was able to prevent liver mitochondrial fragmentation after 18-h CLP (Figure 8A). We then evaluated the effect of the Drp1 inhibitor on mitochondrial functionality and apoptosis. We observed that pretreatment of the animals with mdivi-1 prevented the inhibition of the activity of the ETC complexes (I–III, II and III, and IV) (Figure 8B) and hepatocyte apoptosis (Figure 8C), induced by CLP after 18 h of the procedure.

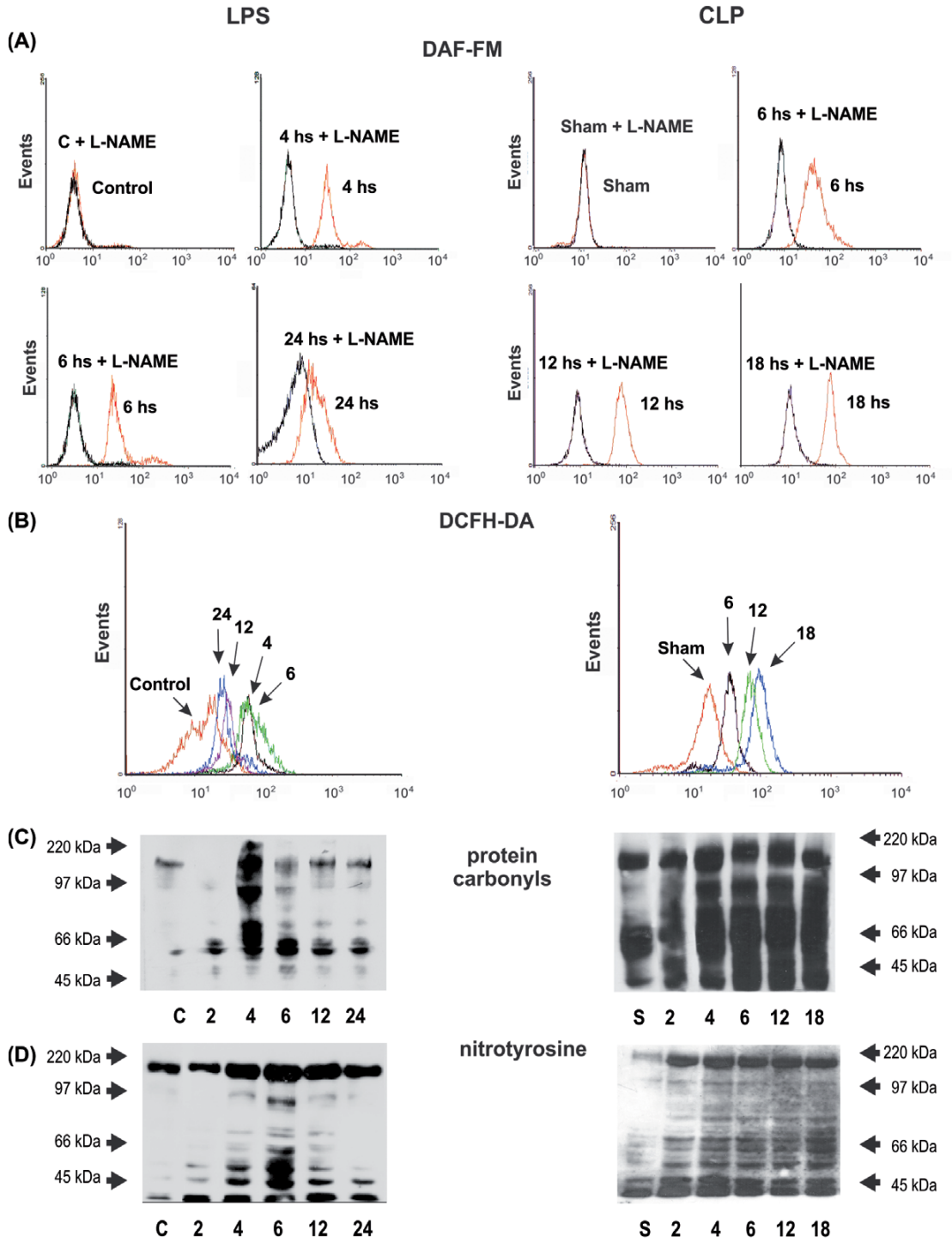

Figure 3. Production of reactive oxygen and nitrogen species in experimental sepsis. (A) Representative flow cytometry histograms of 1 mg/ml of isolated mitochondria incubated with 0.3 mM L-arginine, 10'M DAF-FM and 0.5'M MitoTracker (per duplicate) at 495 nm (excitation) and 515 nm (emission) in the presence or absence of NOS inhibitor (3 mM L-NAME) from $n \geq 3$ for each group. (B) Representative flow cytometry histograms of isolated hepatocytes incubated in phenol red-free DMEM with 5'M DCFH-DA, obtained by duplicate, at 504 nm (excitation) and 529 nm (emission) from $n \geq 3$ for each experimental group. (C) Representative western blot of protein carbonyls obtained from rat liver mitochondria at different times after LPS or CLP treatment from $n \geq 4$ for each group. (D) Representative western blot of nitrated proteins from the different groups; membranes were revealed with anti-3-nitrotyrosine antibodies from $n \geq 4$ for each group.

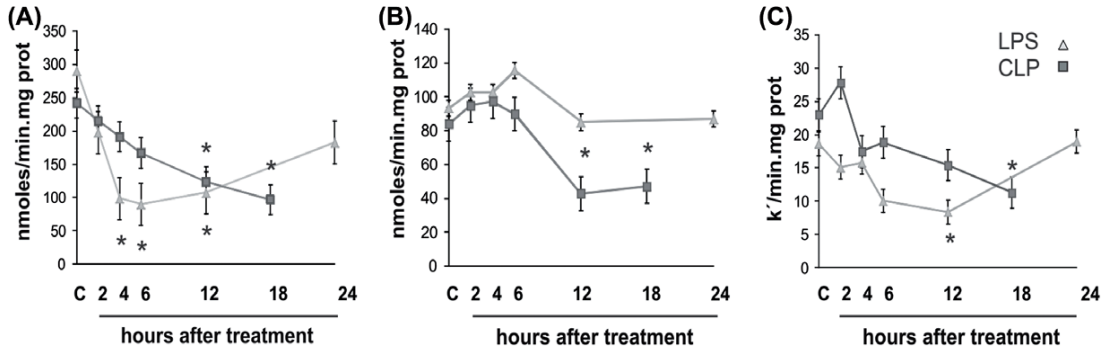

Figure 4. Effects of LPS or CLP treatment on mitochondrial complex activities. Liver mitochondria were isolated, and subjected to three cycles of freeze/thawing (A) Complexes I–III activity was measured following the reduction of cytochrome c at 30°C in the presence of NADH and KCN. (B) Complexes II and III activities, by following the reduction of cytochrome c at 30°C in the presence of potassium succinate. (C) Complex IV activity was assayed by the oxidation of cytochrome c. The reaction rate was measured as the pseudo–first-order reaction constant (k^{I}) and expressed as k^{I}/min. mg protein. Results are expressed as mean ± SEM for 6–8 rats per duplicate, and *represents $p < 0.05$, one-way analysis of variance (ANOVA) and Dunnett's post-hoc test.

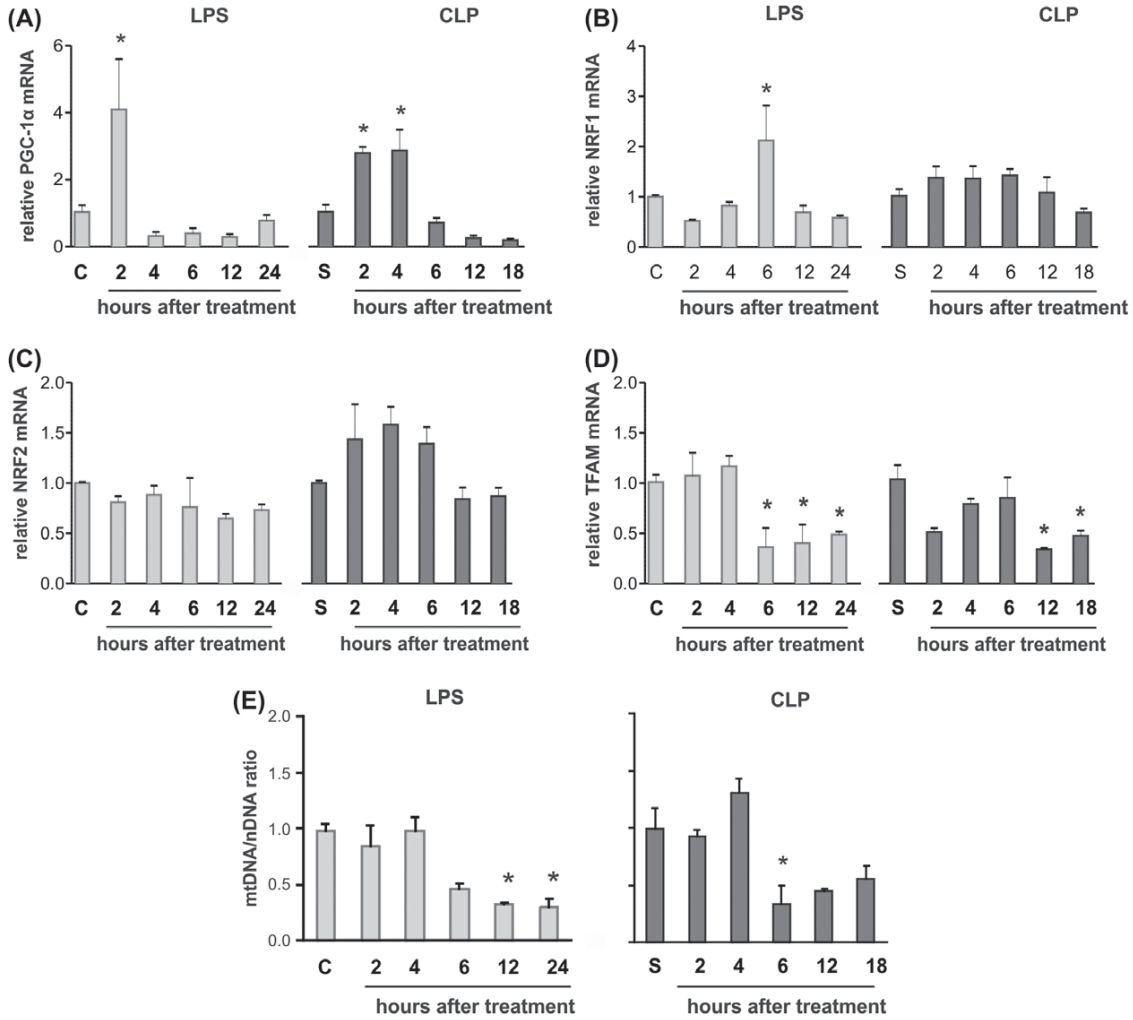

Figure 5. Effects of LPS administration and CLP procedure on mitochondrial biogenesis. (A, B, C, and D) The mRNA levels of PGC-1α, NRF1, NRF2, and Tfam were measured in TRIZOL-treated liver extracts from all the studied groups, β-actin mRNA was used as standard. (E) Quantification of mtDNA and nuclear DNA by qPCR. mtDNA/nDNA ratio was calculated. Results were expressed as the mean ± SEM, $n \geq 5$, per duplicate, and *represents $p < 0.05$, one-way analysis of variance (ANOVA) and Dunnett's post-hoc test.

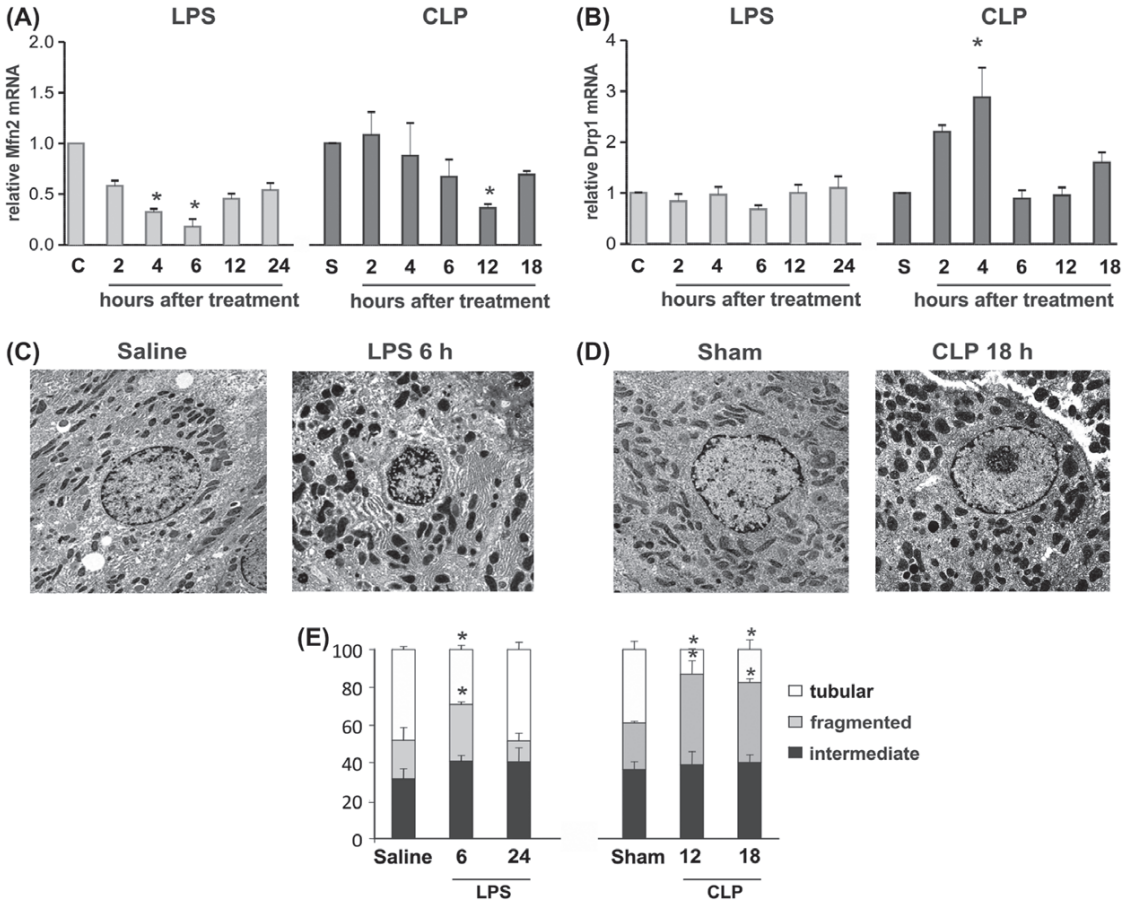

Figure 6. Effects of LPS administration and CLP procedure on mitochondrial dynamics. (A and B) The mRNA levels of the fusion protein Mfn2 and the fission protein Drp1 were measured in TRIZOL-treated liver extracts from all the studied groups using RT-qPCR. Results are expressed as the mean ± SEM, $n \geq 5$ per duplicate. (C and D) Mitochondrial morphology was evaluated using electron microscopy of fixed liver slices from control, sham, LPS 6 h and CLP 18 h groups ($n = 5$ for each experimental group). (Magnification: 3000×). (E) Tubular, fragmented, and intermediate mitochondria were counted per arbitrary area. The percentage distribution of tubular, fragmented, and intermediate hepatocyte mitochondria was determined in a minimum of 8–10 random fields at 3000 × magnification to ensure a representative area of analysis ($n = 5$ for each experimental group). Mitochondria whose length were more than thrice its width were considered tubular; round mitochondria were considered fragmented; while the remaining ones were named intermediate. The analysis was performed by two different investigators in a blinded fashion. *represents $p < 0.05$, one-way analysis of variance (ANOVA), and Dunnett's post-hoc test.

Discussion

The objective of this research was to find out the early events that could play a role in the progression of sepsis and its reversal, for which we studied CLP as an experimental model of progressive, and high-lethality sepsis and endotoxemia, as a limited injury process. We focused on mitochondrial functionality, mainly related to nitric oxide and ROS overproduction; and on mitochondrial biogenesis and dynamics as possible processes involved in sepsis outcome. Our observations demonstrate that mitochondrial fusion to fission imbalance is the event determining differential progression of experimental sepsis. To the best of our knowledge, this is the first study demonstrating that fusion to fission imbalance is linked to a differential progression of sepsis.

The different outcome of sepsis is clearly expressed by survival rates after 12 h of treatment, which show that rats undergoing CLP are significantly more susceptible to die than animals undergoing LPS (Supplementary Figure 1 available online at http://informahealthcare.com/doi/abs/10.3109/10715762.2014.906592), in accord with a marked and progressive alteration of hepatic, renal and muscle biochemical profiles, representative of multiple organ failure.

Inducible NOS is differentially expressed in each experimental situation: while it appeared early in liver cytosol of endotoxemic rats and progressively disappeared after 6 h; in CLP, it almost maintained its maximal expression and activity from 6 to 18 h (Figure 1A and B). iNOS was translocated into mitochondria in both models and was mainly expressed in outer membrane and intermembrane space (Figure 1C). The presence of iNOS in mitochondria was previously observed by us and other groups in diaphragm, liver, lung, and heart [26–28].

Mitochondrial NO levels paralleled iNOS time course in both models (Figure 3) and its overproduction was followed by increased plasma NOx levels (Supplementary

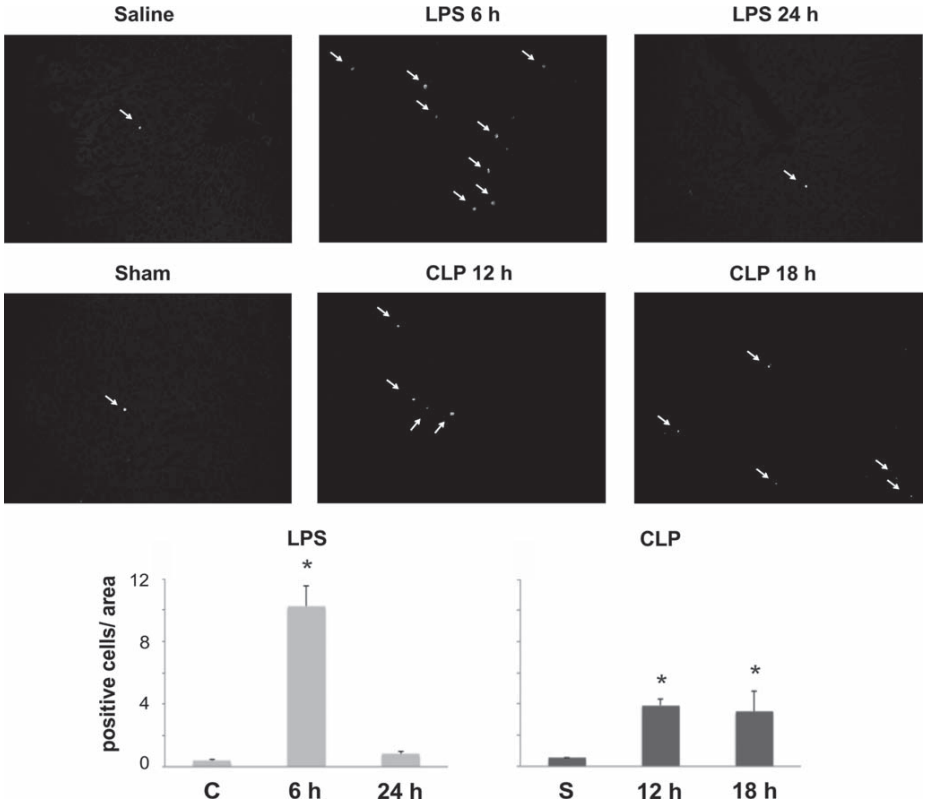

Figure 7. Effects of LPS administration and CLP procedure on liver apoptosis. Apoptosis was evaluated by TUNEL assay in liver slices of control, 6 and 24 h after LPS, and sham, 12 and 18 h after CLP, $n \geq 3$ per duplicate. *represents $p < 0.05$, one-way analysis of variance (ANOVA) and Dunnett's post-hoc test.

Figure 2 available online at http://informahealthcare.com/doi/abs/10.3109/10715762.2014.906592), and increased ROS and nitrogen species (RNS) generation both at mitochondrial and systemic levels.

Increased mitochondrial NO production was mostly generated by inducible NOS, since mitochondrial Ca-dependent NOS activity was unchanged after both treatments (data not shown). Our data are in accord with López et al. [28], which showed in mice diaphragm mitochondria that Ca-dependent activity exhibited no variations at 24 h after CLP, and that the Ca-independent activity was undetectable in the iNOS$^{-/-}$ mice. In contrast to constitutive neuronal NOS, iNOS specific activity was not modified by translocation into mitochondria, as was previously described by Jagnandan et al. by transfection of mitochondria-targeted iNOS constructs to COS-7 cells [29].

Excess ROS and NO production also compromises mitochondrial structure and function through direct oxidation of protein, lipids, and mtDNA, or by generation of peroxynitrite [30]. We and others have previously shown that complex I can be nitrated when mitochondrial NO levels are increased, and that nitration is accompanied by inhibition of its activity [31,32] via a reversible nitrosylation of thiol groups in the complex, or by irreversible nitration [33–37]. On the other hand, substantial carbonylation of specific subunits of mitochondrial respiratory complexes I, III, and V has been shown in chagasic murine hearts infected by *Trypanosoma* cruzi, which presented deficiencies in the activities of the respiratory chain complexes and reduced mitochondrial ATP generation capacity during the course of infection and disease development [38]. We showed herein that alterations in mitochondrial function (evaluated as ETC complex activities) followed the same time course as mitochondrial NO and oxidants production in both experimental models. Moreover, liver mitochondrial dysfunction was parallel to protein nitration and carbonylation, and increased ALT and AST transaminases, markers of hepatocyte injury (Supplementary Table I available online at http://informahealthcare.com/doi/abs/10.3109/10715762.2014.906592). Our results are consistent with previous studies demonstrating liver and skeletal muscle mitochondrial dysfunction during sepsis [26,39–41].

In order to address the reason of the recovery of mitochondrial functionality observed after LPS treatment, we evaluated mitochondrial biogenesis, because previous studies have shown an involvement of this process in the recovery of mitochondrial functions [30]. The protection of mitochondrial integrity and quality is the task of cellular programs that monitor and replace dysfunctional mitochondria with new organelles [16,30,42]. This process of mitochondrial quality control involves a bigenomic program of nuclear- and mitochondrial-encoded gene regulation that rapidly adjusts mitochondrial mass,

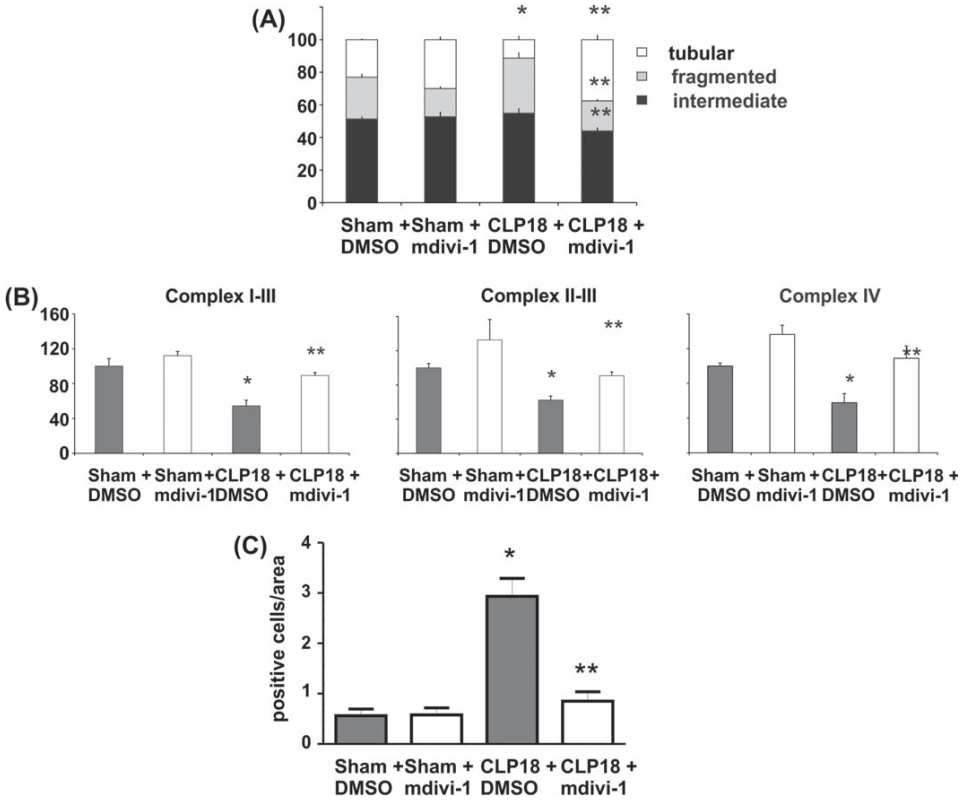

Figure 8. Effects of mdivi-1 on mitochondrial dysfunction and apoptosis. Rats were treated with 50 mg/kg mdivi-1 (dissolved in DMSO) intraperitoneally 1 h prior to sham or CLP procedure and animals were sacrificed at 18 h after surgery (CLP + mdivi-1 and Sham + mdivi-1). Controls of vehicle effect were included (CLP + DMSO and Sham + DMSO). Animals (3-4) were randomly assigned to each experimental group. (A) Examination of mitochondrial fragmentation in liver tissue. Percentage of tubular, fragmented, and intermediate mitochondria per arbitrary area was quantified as in Figure 6. (B) Mitochondrial complex activities measured in isolated liver mitochondria from the four experimental groups in the same conditions described in Figure 4. (C) Apoptosis was evaluated by TUNEL assay by counting positive cells in liver slices of each group, per duplicate. Results are expressed as mean ± SEM for 3–4 rats and *represents $p < 0.05$ respect to sham + DMSO, **represents $p < 0.05$ between CLP + DMSO vs. CLP + mdivi-1 compared using one-way analysis of variance (ANOVA) and Bonferroni post-hoc tests, respectively.

distribution, and phenotype. The program requires the transcription and replication of mitochondrial DNA, mitochondrial protein synthesis, mitochondrial fusion and fission, mitochondrial autophagy, and mitochondrial proliferation, as well as reorganization of the cytoskeleton [42]. Unexpectedly, we found that rat liver mitochondrial biogenesis was not significantly elicited in either experimental model during the first 24 h (Figure 5). There were only slight modifications in PGC-1α and NRF1 transcription factors during early sepsis, mostly in endotoxemia. Actually, Tfam and mtDNA/nDNA content decreased after 6 h of either treatment. These results are in accord with a recent study of Choumar et al. [15], who found that mtDNA was severely damaged after 6–24 h, and just recovered at 48 h after LPS administration, and that liver mtDNA depletion was prevented by inhibiting iNOS activity, scavenging peroxynitrite, or overexpressing MnSOD. On the other hand, Crouser et al. found that liver mitochondrial protein carbonylation was maximal at 24 h after CLP and sustained for more than 48 h, during which time mitochondrial mass was significantly reduced [43]. Therefore, our results showed that mitochondrial biogenesis is not involved in the early recovery of mitochondrial functions seen in endotoxemia, since it was not elicited prior to reversion.

Recently, some studies have shown that interference of either mitochondrial fusion or fission leads to a loss of mtDNA replication [44]. Considering that Mfn2 expression and activity are regulated at transcriptional level, we evaluated Mfn2 mRNA time course and found an 80% decrease at 6 h after endotoxemia, which was partially recovered afterwards; while minimal values were found at 12 h after CLP (Figure 6A). Drp1 mRNA was only modified after CLP, 2–3 fold increase at 2–4 h that was partially sustained at 18 h (Figure 6B). These data show that, in sepsis, the balance between mitochondrial fusion and fission is disrupted either by decreased Mfn2 gene transcription and/or increased Drp1 one. Mitochondrial morphology observed using electron microscopy of liver samples was differentially affected by LPS and CLP. While in LPS-treated animals, fusion (evaluated by the number of elongated mitochondria) was recovered at 24 h; in CLP, mitochondria remained fragmented (evaluated by the number of round mitochondria) at 18 h after treatment. In this sense, we suggest that ROS/RNS overproduction is responsible for this effect, sustained in previous reports

showing that oxidative stress, triggered by NO and/or O_2^-/H_2O_2, increases mitochondrial fragmentation [45–47].

Aside from influencing mitochondrial morphology and the degree of connectivity of mitochondrial networks, mitochondrial fission and fusion proteins can contribute to repair defective mitochondria, to oxidative phosphorylation efficiency, and intramitochondrial calcium signal propagation [48,49]. Chen et al. showed that mitochondrial fusion impairment in skeletal muscle leads to increased mtDNA point mutations and deletions, and a severe defect in respiratory capacity [44]. In this context, complex I is the most affected by DNA mutations since 7 mtDNA-encoded subunits are present in this complex, and complex II is the less compromised because it is coded exclusively by nuclear DNA. These data are in accord with our findings since we observed a more severe decrease of complex I activity than of complex II in both models, which was only affected after 12–18 h of CLP.

The decline of respiratory capacity may lead to the accumulation of mitochondria with low membrane potential and inactivation of the fusion protein OPA1, which is less likely engaged in subsequent fusion events [50]. Moreover, disruption of mitochondrial fusion can result in mitochondrial dysfunction and loss of respiratory capacity, constituting a vicious circle of mitochondrial functionality impairment. During CLP, mitochondria underwent this deleterious feedback mechanism, leading to permanent harm of mitochondrial functionality and dynamics. On the other hand, endotoxemia showed a recovery of both mitochondrial fusion and respiratory capacity, avoiding the vicious circle depicted above. Whether this escape is favored by the limited ROS/RNS generation, or there exists a signal threshold needed to trigger the vicious circle that is not elicited in endotoxemia is still unknown.

Mitochondrial fusion and intermixing of mitochondrial content appear to be a major factor in the maintenance of the bioenergetics state [51], and the loss of this capacity is linked to progressive mitochondrial damage.

Pathologic or experimentally induced imbalance of fusion and fission can also be linked to apoptosis [52]. Morphological changes of mitochondria are closely associated with apoptosis, and Drp1 is essential for the normal progression of apoptosis. We observed that, at maximal NO levels, increased fragmentation was accompanied by apoptosis both at 6 h after LPS and at 12–18 h after CLP, suggesting that fragmentation and mitophagy were not able to rescue the cell from the execution of the program cell death.

Recent evidence demonstrates that mdivi-1 inhibits mitochondrial fission by blocking Drp1 self-assembly and GTP hydrolysis, attenuates apoptosis by inhibiting mitochondrial outer membrane permeabilization, and inhibits cytochrome *c* release during apoptosis [20]. Herein, we observed that inhibition of mitochondrial fission by mdivi-1 administration previous to CLP procedure prevented the inhibition of mitochondrial ETC complexes and hepatocyte apoptosis. These results suggest that mdivi-1 treatment may be a potential therapeutic tool for sepsis.

Conclusions

Endotoxemia and CLP have different time courses of nitric oxide and oxidants production that are followed by differential mitochondrial dysfunction and organ failure with alteration of biochemical markers of tissue damage. It is interesting to note that endotoxemia shows an early and acute liver damage accompanied by cell apoptosis that afterwards is reverted; while CLP procedure shows a more progressive mitochondrial damage that leads to apoptosis and irreversible tissue injury. The recovery of mitochondrial function after 24 h of LPS treatment seemed not to be due to increased mitochondrial biogenesis but instead, to a decreased mitochondrial fragmentation and the recovery of mitochondrial fusion. In contrast, CLP procedure seemed to be a model of progressive damage that is related to the imbalance of mitochondrial fusion and fission.

Acknowledgments

The authors thank Prof Norberto Sanjuan and Margarita López for electron microphotographs.

Declaration of interest

The authors report no declarations of interest. The authors alone are responsible for the content and writing of the paper.

This work was supported by the Agencia Nacional de Promoción Científica y Tecnológica (FONCyT) grant PICT 01625 (to M.C.C.), University of Buenos Aires grant UBACyT M058 and W443 (to J.J.P. and M.C.C.), CONICET grant PIP 0422 (to M.C.C.), and Fundación Pérez Companc, Buenos Aires, Argentina.

References

[1] Dellinger RP, Levy MM, Rhodes A, Annane D, Gerlach H, Opal SM, et al. Surviving Sepsis Campaign: international guidelines for management of severe sepsis and septic shock, 2012. Intensive Care Med 2013;39:165–228.

[2] Dyson A, Singer M. Why does preclinical efficacy fail to translate to the clinical setting? Crit Care Med 2009;37: S30–S37.

[3] Bathia M, He M, Zhang H, Moochhala S. Sepsis as a model of SIRS. Frontiers Biosci 2009;14:4703–4711.

[4] Opal SM. The host response to endotoxin, antilipopolysaccharide strategies, and the management of severe sepsis. Int J Med Microbiol 2007;297:365–377.

[5] Remick DG, Ward PA. Evaluation of endotoxin models for the study of sepsis. Shock 2005;24:7–11.

[6] Hubbard WJ, Choudhry M, Schwacha MG, Kerby JD, Rue LW III, Bland KI, Chaudry IH. Cecal ligation and puncture. Shock 2005;24:52–57.

[7] Beal AL, Cerra FB. Multiple organ failure syndrome in the 1990s. Systemic inflammatory response and organ dysfunction. JAMA 1991;271:226–233.

[8] Kurose I, Miura S, Higuchi H, Watanabe N, Kamegaya Y, Takaishi M, et al. Increased nitric oxide synthase activity as a cause of mitochondrial dysfunction in rat hepatocytes: roles for tumor necrosis factor alpha. Hepatology 1996;24: 1185–1192.

[9] Cawels A. Nitric oxide in shock. Kidney Int 2007;72: 557–565.
[10] Hauser B, Bracht H, Matejovi M, Radermacher P, Venkatesh B. Nitric oxide synthase inhibition in sepsis? Lessons learned from large-animal studies. Anesth Analg 2005;101:488–498.
[11] Fredriksson K, Tjader I, Keller P, Petrovic N, Ahlman B, Schéele C, et al. Dysregulation of mitochondrial dynamics and the muscle transcriptome in ICU patients suffering from sepsis induced multiple organ failure. PLoS One 2008;3:e3686. doi:10.1371/journal.pone.0003686.
[12] Brown GC, Borutaite V. Inhibition of mitochondrial respiratory complex I by nitric oxide, peroxynitrite and S-nitrosothiols. Biochem Biophys Acta 2004;1658:44–49.
[13] Lee HC, Wei YH. Mitochondrial biogenesis and mitochondrial DNA maintenance of mammalian cells under oxidative stress. Int J Biochem Cell Biol 2005;37:822–834.
[14] Rasbach KA, Schnellmann RG. Signaling of mitochondrial biogenesis following oxidative injury. J Biol Chem 2007;282:2355–2362.
[15] Choumar A, Tarhuni A, Lettéron P, Reyl-Desmars F, Dauhoo N, Damasse J, et al. Lypopolysaccharide-induced mitochondrial DNA depletion. Antioxid Redox Signal 2011; 15:2837–2854.
[16] Antico Arciuch VG, Elguero ME, Poderoso JJ, Carreras MC. Mitochondrial regulation of cell cycle and proliferation. Antioxid Redox Signal 2012;16:1150–1180.
[17] Suen DF, Norris KL, Youle RJ. Mitochondrial dynamics and apoptosis. Genes Dev 2008;22:1577–1590.
[18] Chan DC. Fusion and fission: interlinked processes critical for mitochondrial health. Annu Rev Genet 2012;46: 265–287.
[19] Palmer CS, Osellame LD, Stojanovski D, Ryan MT. The regulation of mitochondrial morphology: intrincate mechanisms and dynamic machinery. Cell Signal 2011; 23:1534–1545.
[20] Brooks C, Wei Q, Cho SG, Donq Z. Regulation of mitochondrial dynamics in acute kidney injury in cell culture and rodent models. J Clin Invest 2009;119:1275–1285.
[21] Carreras MC, Converso DP, Lorente AS, Barbich MR, Levisman DM, Jaitovich A, et al. Mitochondrial nitric oxide synthase drives redox signals from proliferation and quiescence in rat liver development. Hepatology 2004; 40:157–166.
[22] Poderoso JJ, Lisdero C, Schöpfer F, Riobó N, Carreras MC, Cadenas E, Boveris A. The regulation of mitochondrial oxygen uptake by redox reactions involving nitric oxide and ubiquinol. J Biol Chem 1999;274:37709–37716.
[23] Berry MN, Friend DS. High-yield preparation of isolated rat parenchymal cells: a biochemical and fine structural study. J Cell Biol 1969;43:506–520.
[24] López-Figueroa M, Caamaño C, Morano MI, Ronn LC, Akil H, Watson SJ. Direct evidence of nitric oxide presence within mitochondria. Biochem Biophys Res Commun 2000;272:129–133.
[25] Morais Cardoso S, Pereira C, Resende Oliveira C. Mitochondrial function is differentially affected upon oxidative stress. Free Rad Biol Med 1999;26:3–13.
[26] Escames G, León J, Macías M, Khaldy H, Acuña-Castroviejo D. Melatonin counteracts lipopolysaccaride-induced expression and activity of mitochondrial nitric oxide synthase in rats. FASEB J 2003;17:932–934.
[27] Lisdero CL, Carreras MC, Meulemans A, Melani M, Aubier M, Boczkowski J, Poderoso JJ. The mitochondrial interplay of ubiquinol and nitric oxide in endotoxemia. Methods Enzymol 2004;382:67–81.
[28] López LC, Escames G, Tapias V, Utrilla P, León J, Acuña-Castroviejo D. Identification of an inducible nitric oxide synthase in diaphragm mitochondria from septic mice: its relation with mitochondrial dysfunction and prevention by melatonin. Int J Biochem Cell Biol 2006;38:267–278.
[29] Jagnandan D, Sessa WC, Fulton D. Intracellular location regulates calcium-calmodulin-dependent activation of organelle-restricted eNOS. Am J Physiol Cell Physiol 2005;289:C1024–C1033.
[30] Piantadosi SA, Suliman HG. Redox regulation of mitochondrial biogenesis. Free Rad Biol Med 2012;53: 2043–2053.
[31] Brealey D, Karyampudi S, Jacques TS, Novelli M, Stidwill R, Taylor V, et al. Mitochondrial dysfunction in a long-term rodent model of sepsis and organ failure. Am J Physiol Regul Integr Comp Physiol 2003;286:R491–497.
[32] Franco MC, Antico Arciuch VG, Peralta JG, Galli S, Levisman D, López LM, et al. Hypothyroid phenotype is contributed by mitochondrial complex I inactivation due to translocated neuronal nitric oxide synthase. J Biol Chem 2006;281:4779–4786.
[33] Beltran B**,** Orsi A**,** Clementi E, Moncada S. Oxidative stress and S-nitrosylation of proteins in cells. Br J Pharmacol 2000;129:953–960.
[34] Borutaite V, Budriunaite A, Brown GC. Reversal of nitric oxide-, peroxynitrite- and S-nitrosothiol-induced inhibition of mitochondrial respiration or complex I activity by light and thiols. Biochim Biophys Acta 2000;1459:405–412.
[35] Riobo NA**,** Clementi E, Melani M, Boveris A, Cadenas E, Moncada S, Poderoso JJ. Nitric oxide inhibits mitochondrial NADH: ubiquinone reductase activity through peroxynitrite formation. Biochem J 2001;359:139–145.
[36] Carreras MC, Franco MC, Peralta JG, Poderoso JJ. Nitric oxide, complex I, and the modulation of mitochondrial reactive species in biology and disease. Mol Aspects Med 2004;25:125–139.
[37] Carreras MC, Poderoso JJ. Mitochondrial nitric oxide in the signaling of cell integrated responses. Am J Physiol Cell Physiol 2007;292:1569–1580.
[38] Dalle-Donne I, Aldini G, Carini M, Colombo R, Rossi R, Milzani A. Protein carbonylation, cellular dysfunction, and disease progression. J Cell Mol Med 2006;10:389–406.
[39] Boczkowski J, Lisdero C, Lanone S, Carreras MC, Boveris A, AubierM, Poderoso JJ. Endogenous peroxynitrite mediates mitochondrial dysfunction in rat diaphragm during endotoxemia. FASEB J 1999;13:1637–1646.
[40] Alvarez S, Boveris A. Mitochondrial nitric oxide metabolism in rat muscle during endotoxemia. Free Rad Biol Med 2004;37:1472–1478.
[41] Protti A, Carré J, Frost MT, Taylor V, Stidwill R, Rudiger A, Singer M. Succinate recovers mitochondrial oxygen consumption in septic rat skeletal muscle. Crit Care Med 2007;35:2150–2155.
[42] Hock MB, Kralli A. Transcriptional control of mitochondrial biogenesis and function. Annu Rev Physiol 2009;71: 177–203.
[43] Crouser ED, Julian MW, Huff JE, Struck J, Cook CD. Carbamoyl phosphate synthase-1: a marker of mitochondrial damage and depletion in the liver during sepsis. Crit Care Med 2006;34:2439–2446.
[44] Chen H, Vermulst M, Wang YE, Chomyn A, Prolla TA, McCaffery JM, Chan DC. Mitochondrial fusion is required for mtDNA stability in skeletal muscle and tolerance of mtDNA mutations. Cell 2010;141:280–289.
[45] Cho DH, Nakamura T, Fang J, Cieplak P, Godzik A, Gu Z, Lipton SA. S-nitrosylation of Drp1 mediates β-amyloid-related mitochondrial fission and neuronal injury. Science 2009;324:102–105.
[46] Foster MW, Hess DT, Stamler JS. Protein S-nitrosylation in health and disease: a current perspective. Trends Mol Med 2009;15:391–404.
[47] Wu S, Zhou F, Zhang Z, Xing D. Mitochondrial oxidative stress causes mitochondrial fragmentation via differential modulation of mitochondrial fission-fusion proteins. FEBS J 2011;278:941–954.

[48] Chen H, Chan DC. Emerging functions of mammalian mitochondrial fusion and fission. Hum Mol Genet 2005; 14:R283–289.
[49] Campello S, Scorrano L. Mitochondrial shape changes: orchestrating cell pathophysiology. EMBO Rep 2010;11: 678–684.
[50] Muster B, Kohl W, Wittig I, Strecker V, Joos F, Haase W, et al. Respiratory chain complexes in dynamic mitochondria display a patchy distribution in life cells. PLoS One 2010;5:e11910. doi:10.1371/journal.pone.0011910
[51] Westermann B. Bioenergetics role of mitochondrial fusion and fission. Biochim Biophys Acta 2012;1817: 1833–1838.
[52] Westermann B. Mitochondrial fusion and fission in cell life and death. Nature Rev Mol Cell Biol 2010;11: 872–884.

Supplementary material available online

Supplementary Figures 1–2 & Table 1.